Article

Combined Convective Energy Transmission Performance of Williamson Hybrid Nanofluid over a Cylindrical Shape with Magnetic and Radiation Impressions

Firas A. Alwawi [1,*] , **Feras M. Al Faqih** [2] , **Mohammed Z. Swalmeh** [3,4] **and Mohd Asrul Hery Ibrahim** [4]

1   Department of Mathematics, College of Sciences and Humanities in Al-Kharj,
    Prince Sattam bin Abdulaziz University, Al-Kharj 11942, Saudi Arabia
2   Department of Mathematics, Al-Hussein Bin Talal University, Ma'an 71111, Jordan
3   Faculty of Arts and Sciences, Aqaba University of Technology, Aqaba 77110, Jordan
4   Faculty of Entrepreneurship and Business, Universiti Malaysia Kelantan,
    Kota Bharu 16100, Kelantan, Malaysia
*   Correspondence: f.alwawi@psau.edu.sa

Abstract: This analysis focuses on extending and developing some previous studies of energy transport through nanofluids to include the states of combined convection flow of a Williamson hybrid nanofluid that flows around a cylinder. Mathematical models that simulate the behavior of these upgraded nanofluids are constructed by expanding the Tiwari and Das model, which are then solved numerically via Keller box approaches. The accuracy of the results is emphasized by comparing them with the previous published outcomes. Nanosolid volume fraction $0 \leq \chi \leq 0.1$, combined convection $-1 \leq \lambda \leq 5$, radiation factor $0.1 \leq R \leq 6$, Weissenberg number $0.2 \leq We \leq 0.9$, and magnetic factor $0.1 \leq M \leq 1$ are the factors that have been taken into consideration to examine the energy transfer performance of Williamson hybrid nanofluid. Numerical and graphical outcomes are obtained using MATLAB, analyzed, and discussed in depth. According to the outcomes, the Weissenberg number reduces energy transfer and friction forces. Both the combined convective coefficient and the radiation factor improved the rate of energy transfer and increased the velocity of the host fluid. The fluid velocity and rate of energy transfer can be reduced by increasing the magnetic factor. The nanoparticle combination of silver and aluminum oxide (Ag-Al_2O_3) has demonstrated superiority in enhancing the energy transfer rate and velocity of the host fluid.

Keywords: Williamson hybrid nanofluid; combined convection; magnetohydrodynamics; thermal radiation; Tiwari and Das model

MSC: 76B99

1. Introduction

Many fluids that play critical roles in energy transmission are not subject to Newton's laws; in other words, the viscosity or flow characteristics of these non-Newtonian fluids are affected not only by temperature or pressure but are also positively or negatively affected by stress. This has led to the emergence of many mathematical models that have tried to predict the behavior of these non-Newtonian fluids. Among the most widely used non-Newtonian models is the Williamson model, which has been constructed by Williamson [1] to simulate the characteristics of the flow of shear-thinning fluids. In the following decades, many studies established their own mathematical models based on the Williamson model, in addition to including many factors that have a great impact on the rate of energy transfer. Nadeem et al. [2] simulated the behavior of the Williamson liquid flowing past a stretching sheet. Nadeem and Hussain [3] examined the energy transport in a Williamson fluid flowing over an exponentially stretching surface. Malik et al. [4,5] presented a numerical

study about the influence of heat generation (absorption) and chemical reactions on energy transmission in Williamson fluid flowing over a stretching cylinder. Iqbal et al. [6] utilized the Shooting Technique to solve the governing model of Williamson liquid flow around an exponentially stretching cylinder. Ogunseye et al. [7] combined the Williamson and Casson models for a flow simulation of the viscoelastic nanoliquid over a vertical moving cylinder. Hussain et al. [8] presented a numerical simulation of the flow of magnetohydrodynamic viscid Williamson using the Buongiorno nanofluid model. Loganathan and Sangeetha [9] conducted a numerical investigation into the energy transfer performance of Williamson nanoliquids. Almaneea [10] investigated the reinforces of mass and heat transmission under thermal changes in Williamson liquid via hybrid nanosolids.

The increasing demand for improving energy transfer through ordinary fluids has led to the invention of several methods to this end. Choi and Eastman's [11] incorporation of the concept of nanofluids into the realm of energy transport for the first time in 1995 was one of the most important methods ever proposed in the field of energy transfer improvement. This was followed by several studies to confirm the effectiveness of these tiny particles and their prominent effect on all factors mainly affecting energy transfer. Studies [12–14] found that nanosolids immersed in liquids at low concentrations (1–5% vol) have the ability to raise the thermal conductivity of the host fluids by more than 20%. Eastman et al. [15] discovered that the inclusion of the nanometal is more efficient in boosting the thermal conductivity of the base liquid than the inclusion of some nanosolid oxides. Other studies, such as Heris et al. [16], were interested in studying the extent of the improvement in the heat transfer coefficient, which is a better indicator than improving the thermal conductivity of nanoliquids employed in some applications, such as designing heat exchange equipment. They found that the rate of improvement in the energy transport coefficient is more than twice the rate of improvement in thermal conductivity. Kuznetsov and Nield [17] conducted a study to expand and improve some of the previous investigations. As a result, many mathematical models have been established that examine all aspects that govern the transfer of energy, including the one-phase model, such as the Tiwari and Das model, which was found to demonstrate the direct impact of the volume fraction of a nanosolid on all physical quantities related to the rate of energy transfer. Many researchers have employed this model, which has proven its efficiency and realism over more than two decades. Tham et al. [18,19], Sheremet and Pop [20], Dogonchi et al. [21], Alwawi et al. [22,23], Hamarsheh et al. [24], Sreedevi and Reddy [25], Khan et al. [26], Jamshed et al. [27], Swalmeh et al. [28,29], and others utilized the Tiwari and Das model to simulate heat transmission problems. The Tiwari and Das model was expanded and developed in this project to examine our problem.

Recently, a new and improved generation of nanomaterials called hybrid nanomaterials has begun to emerge and spread, as they have been synthesized in much experimental research. The main goal of hybrid nanomaterials is to create a nano-compound with integrated features in terms of thermal conductivity, stability, energy transport rate, etc. [30–34]. On the other hand, many numerical studies have been carried out in an attempt to model the behavior of this upgraded nanofluid. Moghadassi et al. [35] confirmed numerically that hybrid nanofluids had the highest values of the heat convection factor as well as a superiority in the Nusselt number when compared to mono-nanofluid. Mehryan [36] employed the finite element technique to solve the governing equation of a square cavity filled with mono-hybrid nanoliquid in the case of mixed convection. Aminian et al. [37] numerically simulate the MHD convection caused by external sources in a cylinder filled with porous media. Alharbi et al. [38] numerically analyzed the thermal performance of mono-hybrid nanoliquid around a cylinder subjected to a magnetic field. Patil and Kulkarni [39] modeled the combined convection flow of magnetized hybrid nanofluid around a slender cylindrical shape. Alwawi et al. [40] reported the characteristic flow of magnetized H_2O/H_2O-ethylene glycol as a host hybrid nano liquid that flows around a cylinder. Patil [41] analyzed the energy transport through a flowing upgrade nanoliquid from a vertical cylindrical surface with a chemical reaction. Williamson hybrid nanofluid flow has also been addressed in recent studies [42–47].

In practice, heat transport via combined convection is important in several engineering and manufacturing implementations. It is clearly visible in electronic cooling systems and nuclear reactors, as well as in food production, solar thermal collectors, etc. On the other hand, magnetohydrodynamics (MHD) has gained prominence and has been the subject of much research due to its ability to control the rate of energy transfer. It can be found in a wide range of applications, including modern metallurgy and metalworking processes, electromagnetic pumps, nuclear reactor cooling, MHD propulsion, and plasma studies. Furthermore, the critical role of thermal radiation as a controlling factor in polymer manufacturing processes, particularly in polymer extrusion, cannot be ignored. Motivated by previous studies that did not address or examine our problem and considering the enormous engineering and industrial applications, the present numerical simulation expands on some previous studies to include the flow of Williamson hybrid nanofluid that flows around a horizontal circular in the case of combined convection under the impact of thermal radiation and magnetism. The impressions of critical factors on physical quantities related to energy transfer are showcased via graphs and tables for the cylindrical surface. It is expected that the current study's findings will not only provide helpful information for future applications but will also provide support for previously published works.

2. Significance of Study

The problem of combined convection flow and heat transfer on a horizontal circular cylinder in Williamson hybrid nanofluids under thermal radiation and magnetic field was studied in this paper. The hybrid nanofluid has attracted the attention of researchers on account of the possibility that hybrid nanofluids may have utility in solving convection problems and improving fluid heat transfer. Hence, nanofluids can enhance the thermal conductivity features between these fluids and the bodies, which is widely accounted for and surveyed in modern mechanical engineering fields. Additionally, this theoretical consideration supplies approximate numerical solutions for testing the thermo-physical influences of the oxides and nanoparticles on Williamson fluids in the presence of combined convection boundary layer flow about a horizontal circular cylinder. It is expected that the outputs gained will contribute to the best understanding of Williamson hybrid nanofluids in the presence of combined flow over a horizontal circular cylinder around the boundary layer area. The problem investigated in this article is resolved numerically by the Matlab coding program, thus the computations aid in the development of computational tools and knowledge that have the capacity to obtain the physical behaviors, such as the effects of thermal radiation on Williamson hybrid nanofluids parameters on the interesting physical quantities. Thus, the development of the software packages may be of assistance to researchers in modeling and simulation.

3. Mathematical Formulations

This section explores the mathematical formulation for the problem of combined convection boundary layer flow in an electro-conductive Williamson hybrid nanofluid. Additionally, a radiative horizontal circular cylinder is considered, and a magnetic field is imposed. The abbreviations for constant wall temperature, gravity vector, and uniform stream velocity are T_w, g, and U_∞, respectively. The observed dimensional variables, $\overline{m}$ and $\overline{n}$, measure the circumference surface and distance perpendicular to the circular cylinder, respectively, see Figure 1.
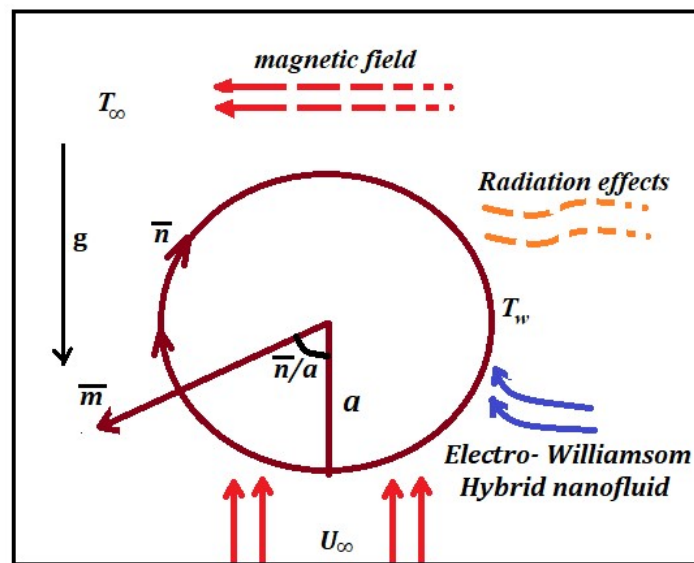
Figure 1. MHD Williamson hybrid nanofluid physical model.

Respecting the above considerations, the dimensional rulings can be written as (see [40,48,49]):

$$\frac{\partial \overline{u}}{\partial \overline{m}} + \frac{\partial \overline{v}}{\partial \overline{n}} = 0 \tag{1}$$

$$\rho_{HNF}\left(\overline{u}\frac{\partial \overline{u}}{\partial \overline{m}} + \overline{v}\frac{\partial \overline{u}}{\partial \overline{n}}\right) = -\frac{\partial \overline{p}}{\partial \overline{m}} + \sqrt{2}v\Gamma\left(\frac{\partial^2 \overline{u}}{\partial \overline{n}^2}\frac{\partial \overline{u}}{\partial \overline{n}}\right) +$$
$$\mu_{HNF}\left(\frac{\partial^2 \overline{u}}{\partial \overline{m}^2} + \frac{\partial^2 \overline{u}}{\partial \overline{n}^2}\right) + \rho_{HNF}\beta_{HNF}g(T - T_\infty)\sin\left(\frac{\overline{m}}{a}\right) - \sigma_{HNF}B_O^2\overline{u}, \tag{2}$$

$$\rho_{HNF}\left(\overline{u}\frac{\partial \overline{u}}{\partial \overline{m}} + \overline{v}\frac{\partial \overline{u}}{\partial \overline{n}}\right) = -\frac{\partial \overline{p}}{\partial \overline{n}} + \sqrt{2}v\Gamma\left(\frac{\partial^2 \overline{u}}{\partial \overline{n}^2}\frac{\partial \overline{u}}{\partial \overline{n}}\right) +$$
$$\mu_{HNF}\left(\frac{\partial^2 \overline{u}}{\partial \overline{m}^2} + \frac{\partial^2 \overline{u}}{\partial \overline{n}^2}\right) + \rho_{HNF}\beta_{HNF}g(T - T_\infty)\cos\left(\frac{\overline{m}}{a}\right) - \sigma_{HNF}B_O^2\overline{u}, \tag{3}$$

$$\overline{u}\frac{\partial T}{\partial \overline{m}} + \overline{v}\frac{\partial T}{\partial \overline{n}} = \alpha_{HNF}\left(\frac{\partial^2 T}{\partial \overline{m}^2} + \frac{\partial^2 T}{\partial \overline{n}^2}\right) - \frac{1}{(\rho c_p)_{HNF}}\frac{\partial Q_R}{\partial \overline{n}}, \tag{4}$$

Whereas the initial profiles, boundary conditions (constant wall temperature) of our study are expressed as [50]:

$$\overline{u} = \overline{v} = 0, \ T = T_w \ at \quad \overline{n} = 0,$$

$$\overline{u} \to \overline{u}_e(\overline{m}), \ T \to T_\infty, \ p \to p_\infty \ at \quad \overline{n} \to \infty, \tag{5}$$

The uniform stream U_∞ flows perpendicular to the cylinder, therefore the free stream velocity $\overline{u}_e(\overline{m}) = U_\infty / \sin(\overline{m}/a)$. The technique for converting dimensional governing equations to non-dimensional equations is done by using non-dimensional variables, which are defined as follows: (see [51]):

$$m = \left(\frac{\overline{m}}{a}\right), n = \mathrm{Re}^{1/2}\left(\frac{\overline{n}}{a}\right), \ u = \left(\frac{u}{U_\infty}\right), v = \left(\frac{\overline{v}}{U_\infty}\right)\mathrm{Re}^{1/2}$$
$$u_e(m) = \frac{\overline{u}_e(\overline{m})}{U_\infty}, \theta = \frac{T - T_\infty}{T_w - T_\infty}, p = \frac{\overline{p} - p_\infty}{\rho_f(U_\infty^2)}. \tag{6}$$

where $\mathrm{Re} = U_\infty a / v_f$ represents the Reynolds number, and the Prandtl number is symbolized by $\mathrm{Pr} = \frac{v_f}{\alpha_f}$. Further, $Q_R = -\frac{4\tau}{3\omega}\frac{\partial T^4}{\partial \overline{n}} = \frac{16\tau}{3\omega}T^3\frac{\partial T}{\partial n}$ is the Rosseland diffusion approximation for radiation, which was proposed by Howell et al. [52], where τ and ω are Stefan–Boltzmann and mean absorption coefficients. Table 1 describes the properties of hybrid nanofluids and mono nanofluids.

Table 1. Properties of mono and hybrid nanoliquids [40,53].

Properties of the Mono Nanofluid	Properties of the Hybrid Nanofluid
$\rho_{MNF} = (1 - \chi_{oxide})\rho_f + \chi_{oxide}\rho_{oxide},$	$\rho_{HNF} = \left(1 - \chi_{Ag}\right)[(1 - \chi_{oxide})\rho_f + \chi_{oxide}\rho_{oxide}] + \chi_{Ag}\rho_{Ag},$
$(\rho c_p)_{MNF} = (1 - \chi_{oxide})(\rho c_p)_f + \chi_{oxide}(\rho c_p)_{oxide},$	$(\rho c_p)_{HNF} =$ $\left(1 - \chi_{Ag}\right)[(1 - \chi_{oxide})(\rho Cp)_f + \chi_{oxide}(\rho Cp)_{oxide}] + \chi_{Ag}(\rho Cp)_{Ag},$
$\beta_{MNF} = (1 - \chi_{oxide})\beta_f + \chi_{oxide}\beta_{oxide}$	$\beta_{HNF} = \left(1 - \chi_{Ag}\right)[(1 - \chi_{oxide})\beta_f + \chi_{oxide}\beta_{oxide}] + \chi_{Ag}\beta_{Ag}.$
$\mu_{MNF} = \dfrac{\mu_f}{(1-\chi_{oxide})^{2.5}},$	$\mu_{HNF} = \dfrac{\mu_f}{\left(1-\chi_{Ag}\right)^{2.5}(1-\chi_{oxide})^{2.5}},$
$\dfrac{k_{MNF}}{k_f} = \dfrac{\left(k_{oxide}+2k_f\right)-2\chi_{oxide}\left(k_f-k_{oxide}\right)}{\left(k_{oxide}+2k_f\right)+\chi_{oxide}\left(k_f-k_{oxide}\right)},$	$\dfrac{k_{HNF}}{k_{bf}} = \dfrac{k_{Ag}+2k_{bf}-2\chi_{Ag}\left(k_{bf}-k_{oxide}\right)}{k_{Ag}+2k_{bf}+\chi_{Ag}\left(k_{bf}-k_{oxide}\right)},\ \dfrac{k_{bf}}{k_f} = \dfrac{k_{Ag}+2k_f-2\chi_{Ag}\left(k_f-k_{Ag}\right)}{k_{Ag}+2k_f+\chi_{Ag}\left(k_f-k_{Ag}\right)},$
$\alpha_{MNF} = \dfrac{k_{MNF}}{(\rho c_p)_{MNF}},$	$\alpha_{HNF} = \dfrac{k_{HNF}}{(\rho cp)_{HNF}},$
$\dfrac{\sigma_{MNF}}{\sigma_f} = 1 + \dfrac{3(\sigma-1)\chi_{oxide}}{(\sigma+2)-(\sigma-1)\chi_{oxide}},\ \ \sigma = \dfrac{\sigma_{oxide}}{\sigma_f}$	$\dfrac{\sigma_{HNF}}{\sigma_{bf}} = \left[\dfrac{\sigma_{Ag}+2\sigma_{bf}-2\chi_{Ag}(\sigma_{bf}-\sigma_{Ag})}{\sigma_{Ag}+2\sigma_{bf}+\chi_{Ag}(\sigma_{bf}-\sigma_{Ag})}\right],\ \dfrac{\sigma_{bf}}{\sigma_f} = \left[\dfrac{\sigma_{oxide}+2\sigma_f-2\chi_{oxide}(\sigma_f-\sigma_{oxide})}{\sigma_{oxide}+2\sigma_f+\chi_{oxide}(\sigma_f-\sigma_{oxide})}\right]$

In the case of a combined convection hybrid nanofluid, Equations (6) and the thermo-physical properties in Table 1 would be substituted. Likewise, it can use the advantageous boundary layer approximation technique (Re→∞), to determine $(-\partial P/\partial m) = (\partial u_e/\partial m)$ and $(\partial P/\partial n) = 0$ (see [51]). That is, the equations that govern radiation influences on electro-conductive Williamson hybrid nanofluid with the magnetic field are:

$$\frac{\partial u}{\partial m} + \frac{\partial v}{\partial n} = 0 \tag{7}$$

$$u\frac{\partial u}{\partial m} + v\frac{\partial u}{\partial n} = u_e\frac{\partial u_e}{\partial m} + \frac{\rho_f}{\rho_{HNF}}\left(\frac{1}{(1-\chi_{Ag})^{2.5}(1-\chi_{oxide})^{2.5}}\right)\frac{\partial^2 u}{\partial n^2} + \mathrm{We}\left(\frac{\partial^2 u}{\partial n^2}\frac{\partial u}{\partial n}\right)$$
$$+\frac{1}{\rho_{HNF}}\left(\left(1-\chi_{Ag}\right)[(1-\chi_{oxide})\rho_f + \chi_{Ag}\frac{\rho_{Ag}\beta_{Ag}}{\beta_f}] + \chi_{oxide}\frac{\rho_{oxide}\beta_{oxide}}{\beta_f}\right)\lambda\theta\sin m \ - \ \frac{\rho_f}{\rho_{HNF}}\frac{\sigma_{HNF}}{\sigma_f}\mathrm{M}u, \tag{8}$$

$$\left(\frac{\mathrm{Pr}}{1+(3/4)\mathrm{R}}\right)\left(u\frac{\partial\theta}{\partial m} + v\frac{\partial\theta}{\partial n}\right)$$
$$= \left[\frac{k_{HNF}/k_f}{(1-\chi_{Ag})[(1-\chi_{oxide})+\chi_{oxide}(\rho Cp)_{oxide}/(\rho Cp)_f]+\chi_{Ag}(\rho Cp)_{Ag}/(\rho Cp)_f}\right]\frac{\partial^2\theta}{\partial n^2}, \tag{9}$$

which is equivalent to $\mathrm{We} = \frac{\Gamma\eta\,\mathrm{Gr}^{3/4}}{a^3}$, $\mathrm{M} = \left(\frac{\sigma_f B_0^2 a^2 \mathrm{Gr}^{-1/2}}{\rho_f v_f}\right)$, $\lambda = \frac{\mathrm{Gr}}{\mathrm{Re}^2}$ where We, M and λ are the Weissenberg number, the magnetic parameter, and the mixed convection parameter. Furthermore, by replacing the properties given in Table 1 and Equation (6), we yield the following non-dimensional boundary conditions

$$\begin{aligned} u = v = 0, \ \ \theta = 1, \ \text{at} \ n = 0, \\ u \to 0, \ \ \theta \to 0, p \to 0, \ \text{as} \ n \to \infty. \end{aligned} \tag{10}$$

Let's now reduce the system (7)–(10) using the procedure of transformation variables, which are defined as: (see [7])

$$\psi = mf(m,n), \ \ \theta = \theta(m,n), \tag{11}$$

$$u = \frac{\partial\psi}{\partial m} \ \text{and} \ v = -\frac{\partial\psi}{\partial n} \tag{12}$$

where ψ is called the stream function.

By exploiting the transformation variables (11) and (12), the non-dimensional governing equations are reduced into the following partial differential equations:

$$\frac{\rho_f}{\rho_{HNF}}\left(\frac{1}{(1-\chi_{Ag})^{2.5}(1-\chi_{oxide})^{2.5}}\right)\frac{\partial^3 f}{\partial n^3} + \text{We}\frac{\partial^3 f}{\partial n^3}\frac{\partial^2 f}{\partial n^2} + f\frac{\partial^2 f}{\partial n^2} - \left(\frac{\partial f}{\partial n}\right)^2 +$$
$$\frac{1}{\rho_{HNF}}\left((1-\chi_{Ag})[(1-\chi_{oxide})\rho_f + \chi_{oxide}\frac{\rho_{oxide}\beta_{oxide}}{\beta_f}] + \chi_{Ag}\frac{\rho_{Ag}\beta_{Ag}}{\beta_f}\right)\lambda\frac{\sin n}{n}\ \theta \tag{13}$$
$$-\frac{\rho_f}{\rho_{HNF}}\frac{\sigma_{HNF}}{\sigma_f}\text{M}\ \frac{\partial f}{\partial n} = m\left(\frac{\partial f}{\partial n}\frac{\partial^2 f}{\partial m\partial n} - \frac{\partial f}{\partial m}\frac{\partial^2 f}{\partial n^2}\right)$$

$$\left[\frac{k_{HNF}/k_f}{(1-\chi_{Ag})[(1-\chi_{oxide})+\chi_{oxide}(\rho Cp)_{oxide}/(\rho Cp)_f]+\chi_{Ag}(\rho Cp)_{Ag}/(\rho Cp)_f}\right]\frac{\partial^2\theta}{\partial n^2}$$
$$+\left(\frac{\text{Pr}}{1+(3/4)\text{R}}\right)f\frac{\partial\theta}{\partial n} = m\left(\frac{\partial f}{\partial n}\frac{\partial\theta}{\partial m} - \frac{\partial f}{\partial m}\frac{\partial\theta}{\partial n}\right), \tag{14}$$

Subject to:

$$f = \frac{\partial f}{\partial n} = 0, \theta = 1 \ \text{ at }\ n = 0,$$
$$\frac{\partial f}{\partial n} \to 0,\ \ \theta \to 0,\ \text{ as }\ n \to \infty. \tag{15}$$

In the case of $m \approx 0$, Equations (13)–(15) are determined at the stagnation points. This results in

$$\frac{\rho_f}{\rho_{HNF}}\left(\frac{1}{(1-\chi_{Ag})^{2.5}(1-\chi_{oxide})^{2.5}}\right)\frac{\partial^3 f}{\partial n^3} + \text{We}\frac{\partial^3 f}{\partial n^3}\frac{\partial^2 f}{\partial n^2} + f\frac{\partial^2 f}{\partial n^2} - \left(\frac{\partial f}{\partial n}\right)^2 +$$
$$\frac{1}{\rho_{HNF}}\left((1-\chi_{Ag})[(1-\chi_{oxide})\rho_f + \chi_{oxide}\frac{\rho_{oxide}\beta_{oxide}}{\beta_f}] + \chi_{Ag}\frac{\rho_{Ag}\beta_{Ag}}{\beta_f}.\right)\theta \tag{16}$$
$$-\frac{\rho_f}{\rho_{HNF}}\frac{\sigma_{HNF}}{\sigma_f}\text{M}\ \frac{\partial f}{\partial n} = 0,$$

$$\frac{1}{\text{Pr}}\left[\frac{k_{HNF}/k_f}{(1-\chi_{Ag})[(1-\chi_{oxide})+\chi_{oxide}(\rho Cp)_{oxide}/(\rho Cp)_f]+\chi_{Ag}(\rho Cp)_{Ag}/(\rho Cp)_f}\right]\frac{\partial^2\theta}{\partial n^2}$$
$$+\left(\frac{\text{Pr}}{1+(3/4)\text{R}}\right)f\frac{\partial\theta}{\partial n} = 0 \tag{17}$$

With the boundary conditions

$$f(0,n) = f'(0,n) = 0,\ \theta(0,n) = 1 \ \text{ as }\ n = 0,$$
$$f'(0,n) \to 0,\ \ \theta(0,n) \to 0 \ \text{ as } n \to \infty, \tag{18}$$

In a similar fashion [54], the physical groups highlighted in this analysis are Nusselt number Nu, and skin friction C_f, which coincide with the expressions

$$C_f = \left(\frac{\tau_w}{\rho_f U_\infty^2}\right),\ Nu = \left(\frac{aq_w}{k_f(T_w - T_\infty)} + Q_R\right), \tag{19}$$

where

$$\tau_w = \mu_{HNF}\left(\frac{\partial\overline{u}}{\partial\overline{n}} + \left[\frac{\Gamma}{\sqrt{2}}\left(\frac{\partial\overline{u}}{\partial\overline{n}}\right)^2\right]\right)_{\overline{n}=0}, q_w = -k_{HNF}\left(\frac{\partial T}{\partial\overline{n}}\right)_{\overline{n}=0} \tag{20}$$

Using Equations (6) and (10), C_f and Nu are rewritten as

$$C_f = \text{Gr}^{-1/4}\frac{1}{(1-\chi_{Ag})^{2.5}(1-\chi_{oxide})^{2.5}}m\left(\frac{\partial^2 f}{\partial n^2}(\eta,0) + \frac{\text{We}}{2}\left(\frac{\partial f}{\partial n}(m,0)\right)^2\right),$$

$$Nu = -\text{Gr}^{1/4}\left(1 + \frac{4}{3}R\right)\frac{k_{HNF}}{k_f}\frac{\partial\theta}{\partial n}(m,0), \tag{21}$$

All parameters and symbols are presented in the nomenclature list.

4. Numerical Method

The numerical method utilized in this study is called the Keller box method. This method appears to be efficient with respect to the common numerical methods, and regardless of the recent progress in other methods, it attains strong and very accurate approximations for boundary layer convection problems. In addition, it is also flexible to solve equations in different orders and without restrictions on the numerical solutions (Cebeci and Bradshaw [55]). The Keller box scheme is briefly explained as follows: The partial differential Equations (16) to (18) are reduced to a first-order system via the finite difference scheme. After that, we apply the central differences method to get the finite difference equations. And then, we use Newton's method to linearize the resulting finite difference equations, and it is most appropriate to write them in matrix-vector form because this form will be solved by the block tri-diagonal elimination technique to get the most recently calculated data. Thermo-physical characteristics of the considered nanoparticles and water as a host fluid are given in Table 2. Additionally, Table 3 displayed the local skin friction comparison values with published results investigated by Nazar et al. [56] (the results are in parentheses). Hence, the new outcomes are in good agreement.

Table 2. Thermo-physical characteristics of base fluids and nanoparticles [23,57,58].

Material	ρ (kg/m^3)	C_p (J/kgK)	K (W/mK)	$B \times 10^{-5}$ (K^{-1})	σ (s/m)	Pr
Water	997.1	4179	0.613	21	5.5×10^{-6}	6.2
Ag	10,500	235	429	1.89	6.3×10^{7}	...
Al$_2$O$_3$	3970	765	40	0.85	3.5×10^{7}	...
SiO$_2$	2220	745	1.38	0.055	10^{-21}	...

Table 3. The comparison values of C_f for $\chi_{Ag} = \chi_{Oxide} = 0, We = 0, M = 0, R = 0$, Pr = 6.8, and various values of λ.

m	λ							
	−2.5	−1.5	−1.0	−0.5	0.0	1.0	1.84	1.85
0º	0.0000 (0.0000)	0.0000 (0.0000)	0.0000 (0.0000)	0.0000 (0.0000)	0.0000 (0.0000)	0.0000 (0.0000)	0.0000 (0.0000)	0.0000 (0.0000)
0.2	0.0222 (0.0226)	0.1236 (0.1254)	0.1661 (0.1672)	0.2037 (0.2058)	0. 2398 (0.2421)	0.3081 (0.3099)	0.3626 (0.3630)	0.3627 (0.3637)
0.4		0.2234 (0.2243)	0.3077 (0.3093)	0.3862 (0.3872)	0.4591 (0.4601)	0.5946 (0.5954)	0.6988 (0.7012)	0.6990 (0.7024)
0.6		0.2693 (0.2721)	0.4011 (0.4045)	0.5192 (0.5234)	0.6323 (0.6334)	0.8348 (0.8358)	0.9890 (0.9932)	0.9945 (0.9950)
0.8			0.4287 (0.4329)	0.5958 (0.5968)	0.7427 (0.7453)	1.0135 (1.0146)	1.2195 (1.2220)	1.2239 (1.2244)
1.0			0.3741 (0.3749)	0.5927 (0.5939)	0.7833 (0.7840)	1.1189 (1.1203)	1.3741 (1.3756)	1.3762 (1.3785)
1.2				0.5025 (0.5037)	0.7387 (0.7431)	1.1138 (1.1480)	1.4454 (1.4487)	1.4452 (1.4521)
1.4				0.3068 (0.3074)	0.6174 (0.6209)	1.0977 (1.0994)	1.4359 (1.4425)	1.4446 (1.4464)
1.6					0.4146 (0.4150)	0.9783 (0.9829)	1.3636 (1.3648)	1.3674 (1.3691)
1.8					0.0581 (0.0591)	0.8082 (0.8124)	1.2264 (1.2290)	1.2261 (1.2335)
2.0						0.6044 (0.6061)	1.0487 (1.0525)	1.0551 (1.0573)
2.2						0.3698 (0.3847)	0.8533 (0.8552)	0.8591 (0.8601)
2.4							0.6555 (0.6566)	0.6588 (0.6614)
2.6							0.4676 (0.4728)	0.4771 (0.4772)
2.8							0.2860 (0.3130)	0.3011 (0.3167)
3.0								0.1887 (0.1895)
3.14								0.2062 (0.2097)

5. Results and Discussion

Graphical representations of the impression of various critical factors on physical groups related to heat transport are elaborated in Figures 2–16. The behavior of a Williamson

hybrid nanofluid resulting from exposure to these factors is also discussed and analyzed. Nanosolid volume fraction χ, combined convection λ, radiation factor R, Weissenberg number We, and magnetic factor M are the factors that have been taken into consideration, in which their ranges are $0 \leq \chi \leq 1$, $-1 \leq \lambda \leq 4$, $0.1 \leq R \leq 6$, $0.2 \leq We \leq 0.9$, and $0.1 \leq M \leq 1$. Figures 2 and 3 display how the Weissenberg number We affects the Nusselt number and skin friction. As shown in Figure 2, the rate of energy transport is suppressed in response to a rise in the Weissenberg number. Similarly, as shown in Figure 3, the drag forces are reduced due to this rise. The growth in relaxation time as the number of Weissenberg increases could be causing this behavior. Figures 4 and 5 show how the reaction of the Nusselt number and skin friction with an increase in the radiation factor. As the radiation factor R values grow, additional heat is gained by the Williamson hybrid nanofluid, which enhances the transfer of energy through it and increases the skin friction. Figures 6 and 7 depict how the Nusselt number and skin friction respond to rising values of the combined convection factor λ. As can be seen, the effect of the increase in the combined convection factor on both the Nusselt number and the skin friction is positive, as its values increase, so do the Nusselt number and the skin friction. The cause of this behavior is the growth in buoyant forces caused by rising combined convection factor values. Figures 8 and 9 are plotted to show the impact of magnetic factor on Nusselt number and skin friction. Both the Nusselt number and skin friction are observed to reduce as the strength of the magnetic field intensifies. This phenomenon can be explained by the creation of the Lorentz force as a result of passing a magnetic field through electrically conductive moving fluids, which inhibits both the rate of energy transport and the drag forces. Figures 10 and 11 show the significant effect of the volume fraction of silver nanosolid on energy transfer and skin friction. It is concluded through these plots that growing χ_{Ag} improves heat transmission and reduces skin friction. It is well known that the growth in nanosolid volume fraction leads to an enhancement in the thermal conductivity of the Williamson host fluid, hence an augmentation in Nusselt number and a decrement in skin friction occur.
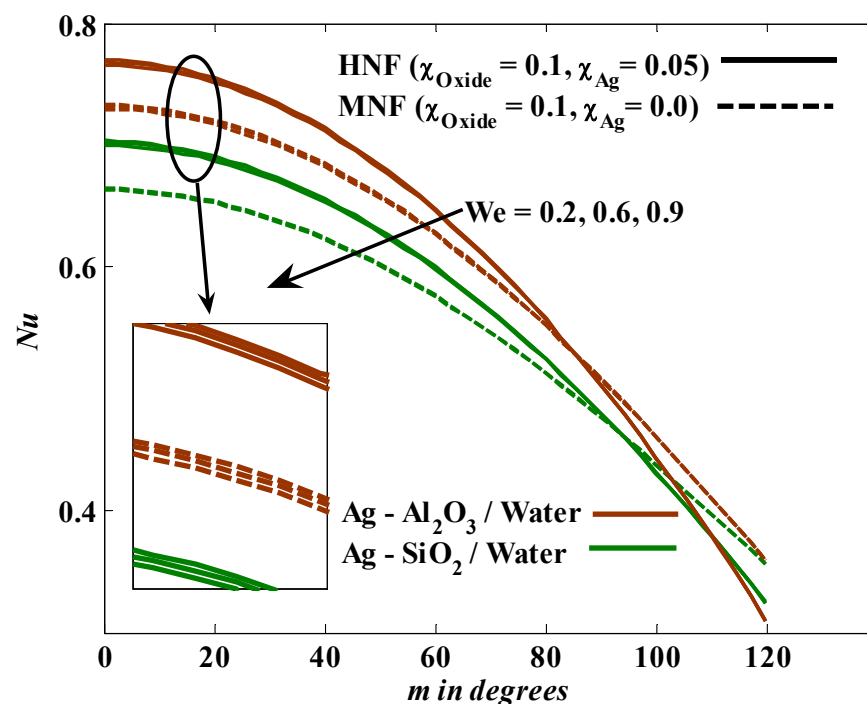

Figure 2. Illustration of We versus Nusselt number at fixed values of $R = 0.2$, $\lambda = 0.1$, & $M = 1$.
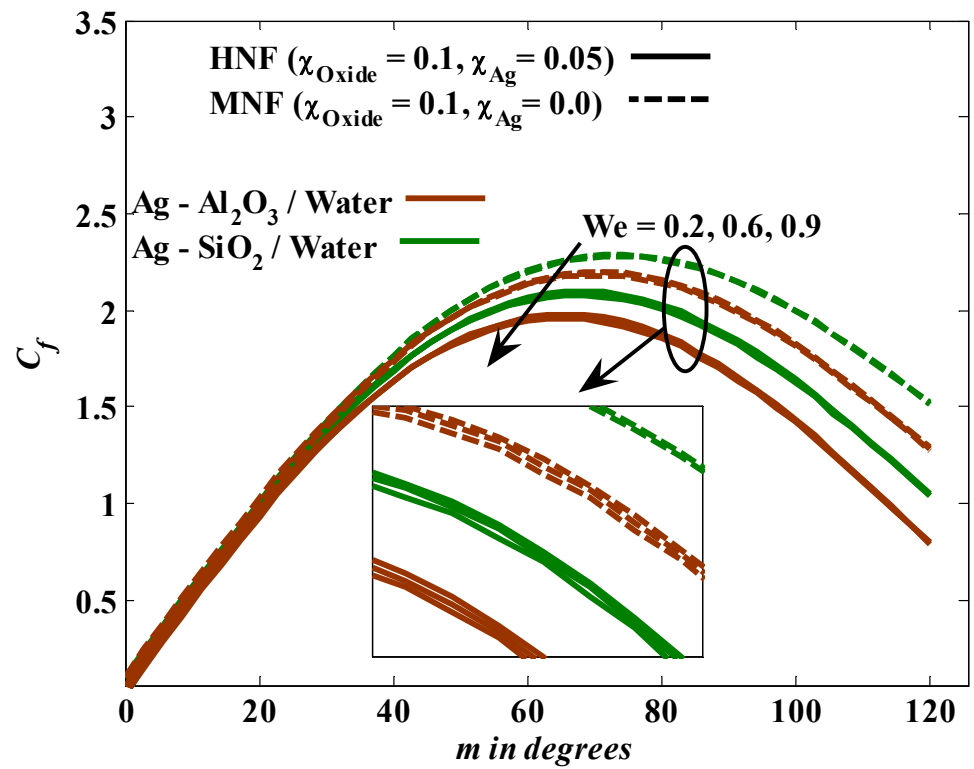
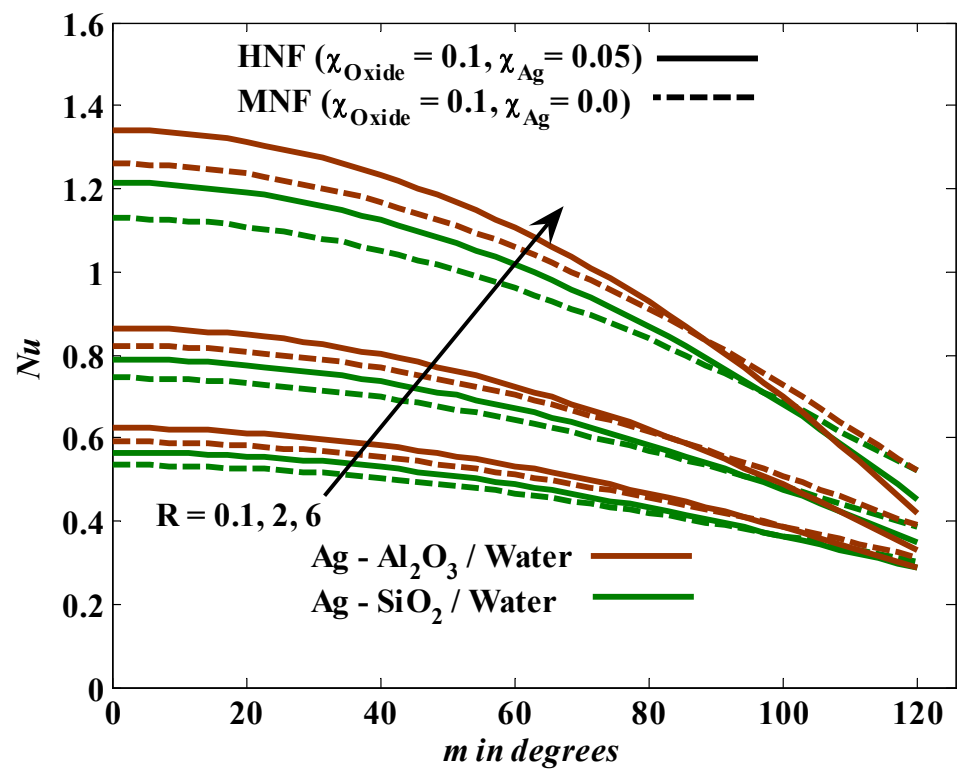**Figure 3.** Illustration of *We* versus skin friction at fixed values of $\lambda = 0.2$, $R = 0.1$, & $M = 1$.

Figure 4. Illustration of *R* versus Nusselt number at fixed values of $We = 0.2$, $\lambda = 0.1$, & $M = 1$.
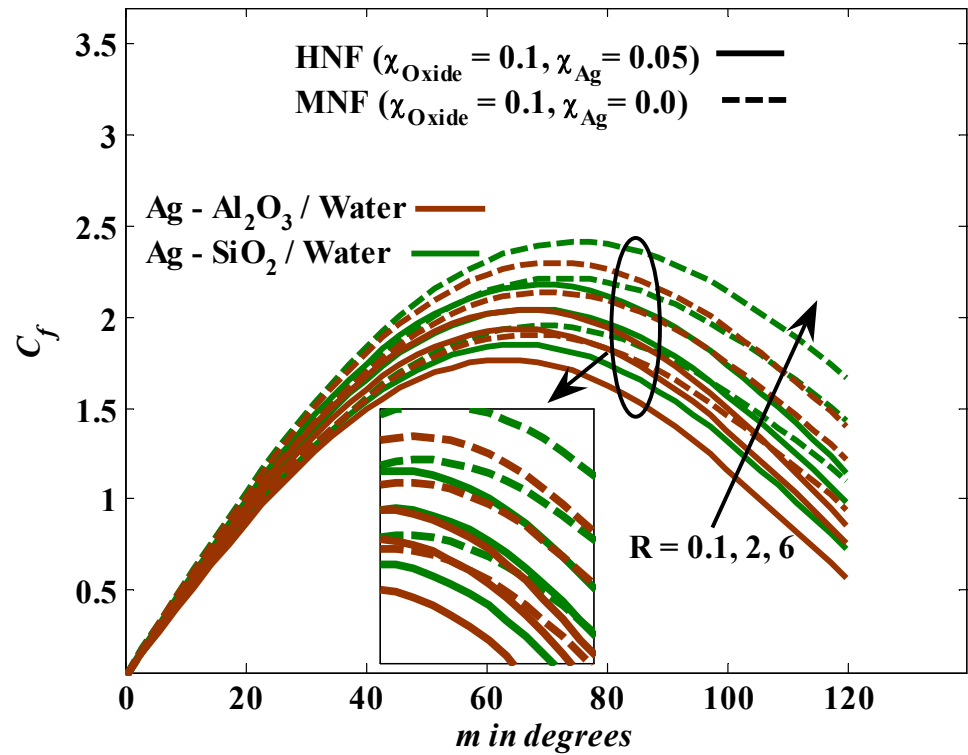
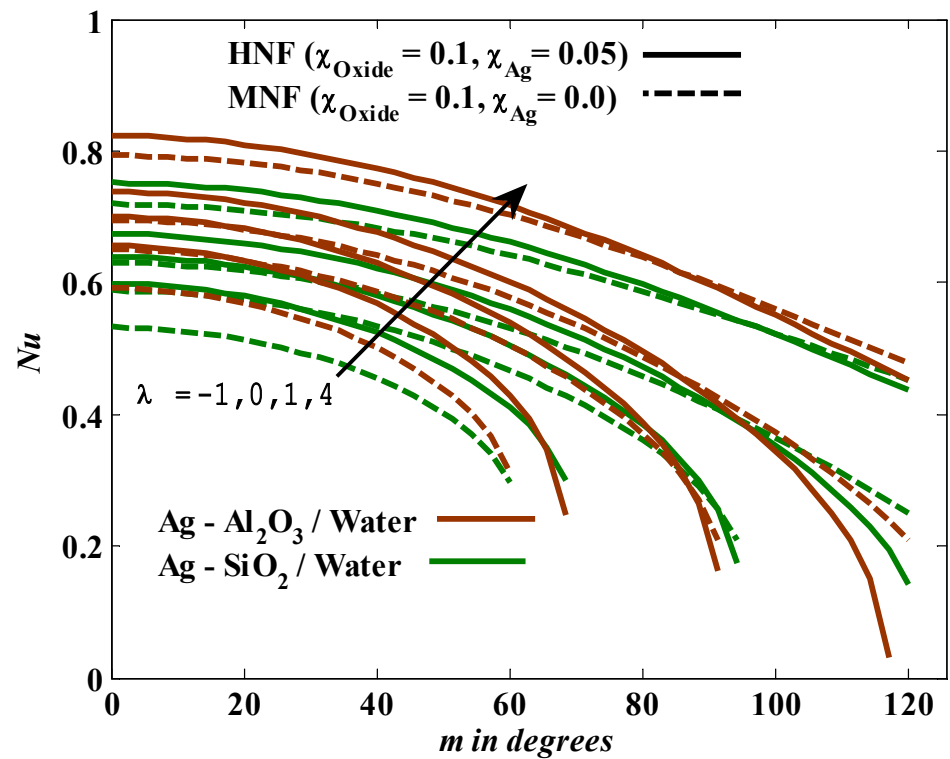**Figure 5.** Illustration of R versus skin friction at fixed values of $We = 0.2$, $\lambda = 0.1$, & $M = 1$.

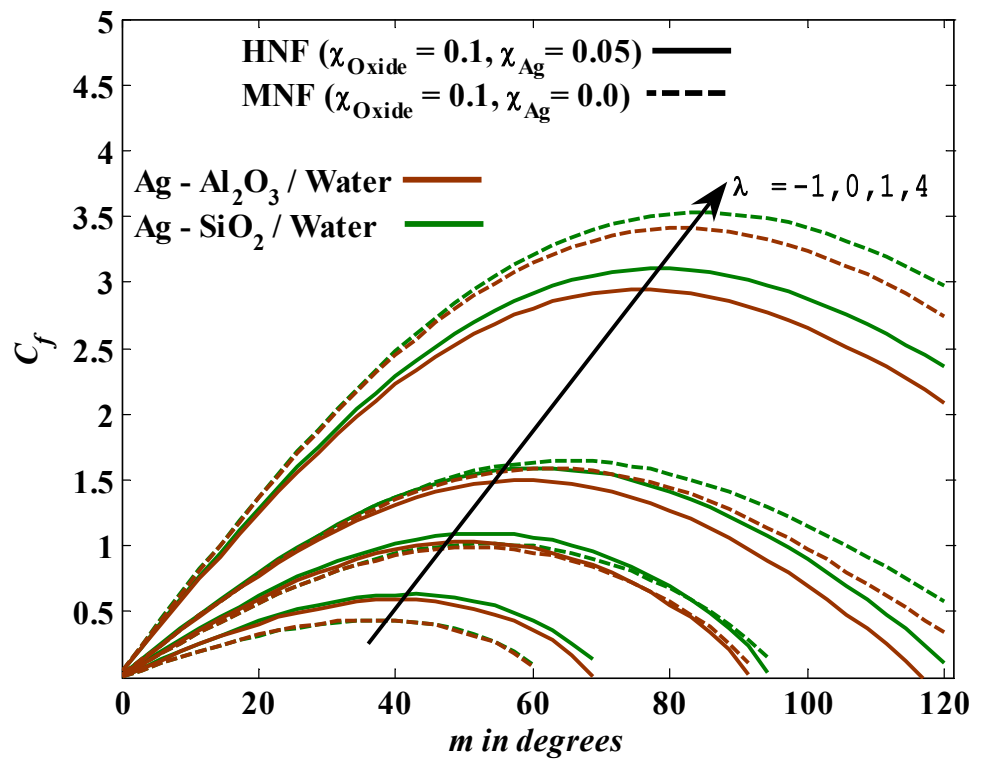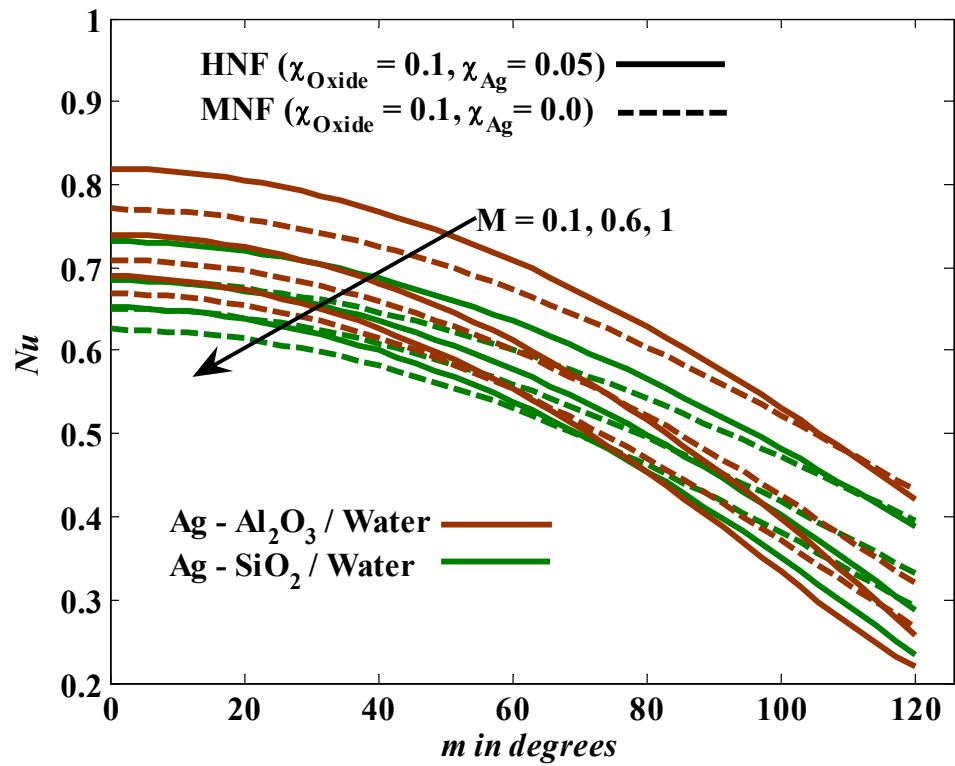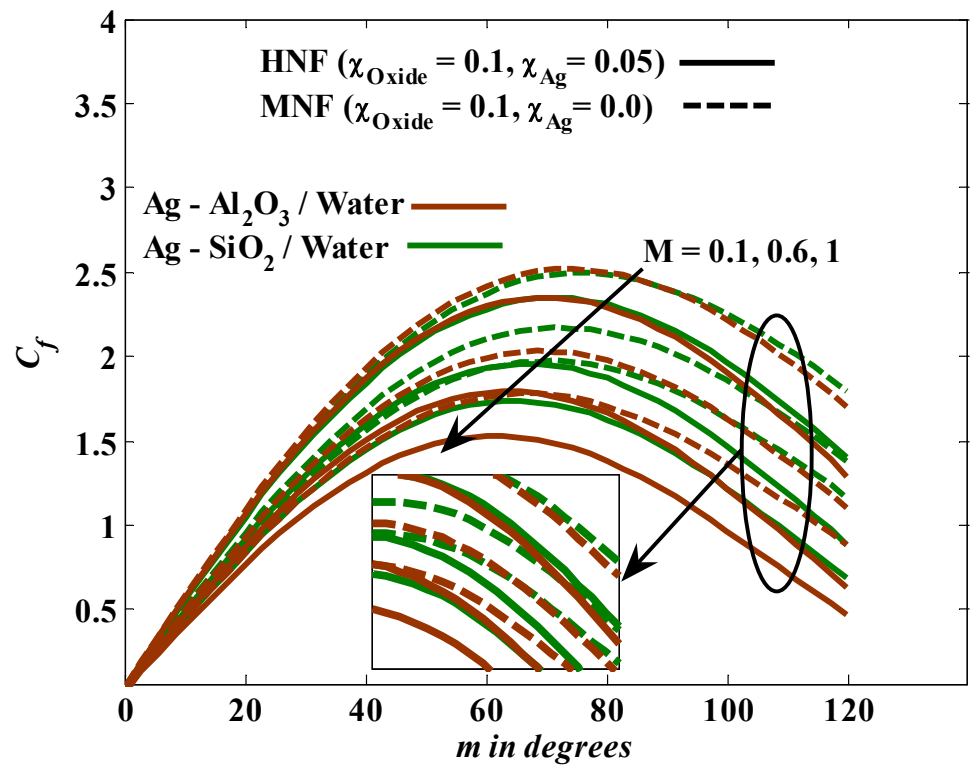**Figure 6.** Illustration of λ versus Nusselt number at fixed values of $We = 0.2$, $R = 0.1$, & $M = 1$.

Figure 7. Illustration of λ versus skin friction at fixed values of $We = 0.2$, $R = 0.1$, & $M = 1$.

Figure 8. Illustration of M versus Nusselt number at fixed values of $We = 0.2$, $\lambda = 0.1$, & $R = 1$.

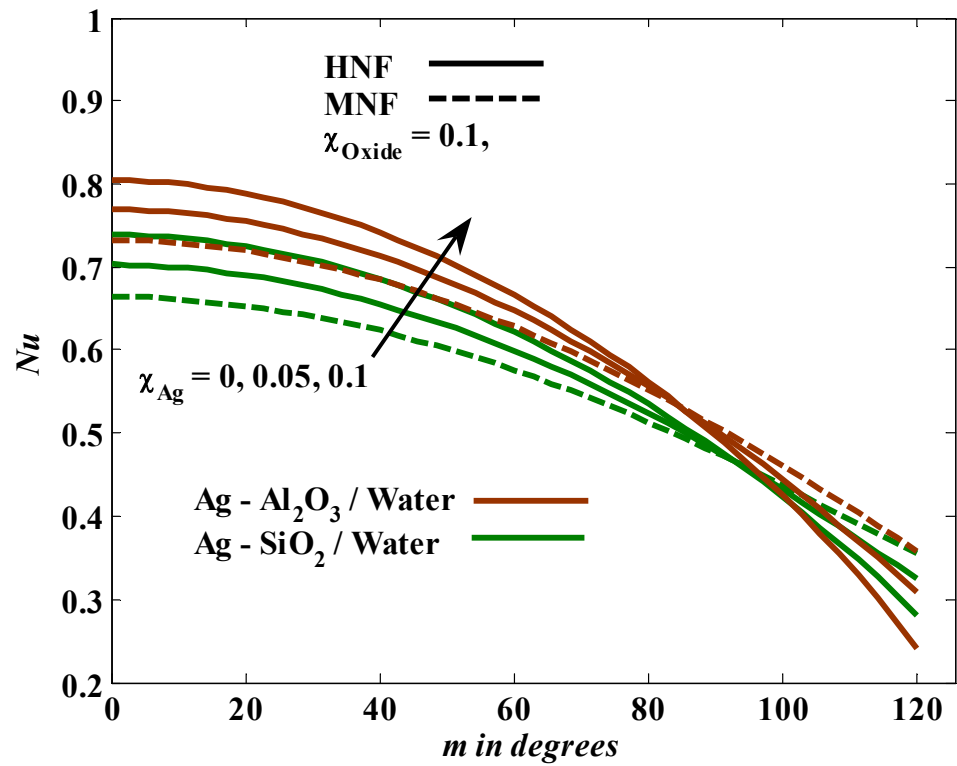**Figure 9.** Illustration of *M* versus skin friction at fixed values of $We = 0.2$, $R = 0.1$, & $\lambda = 1$.
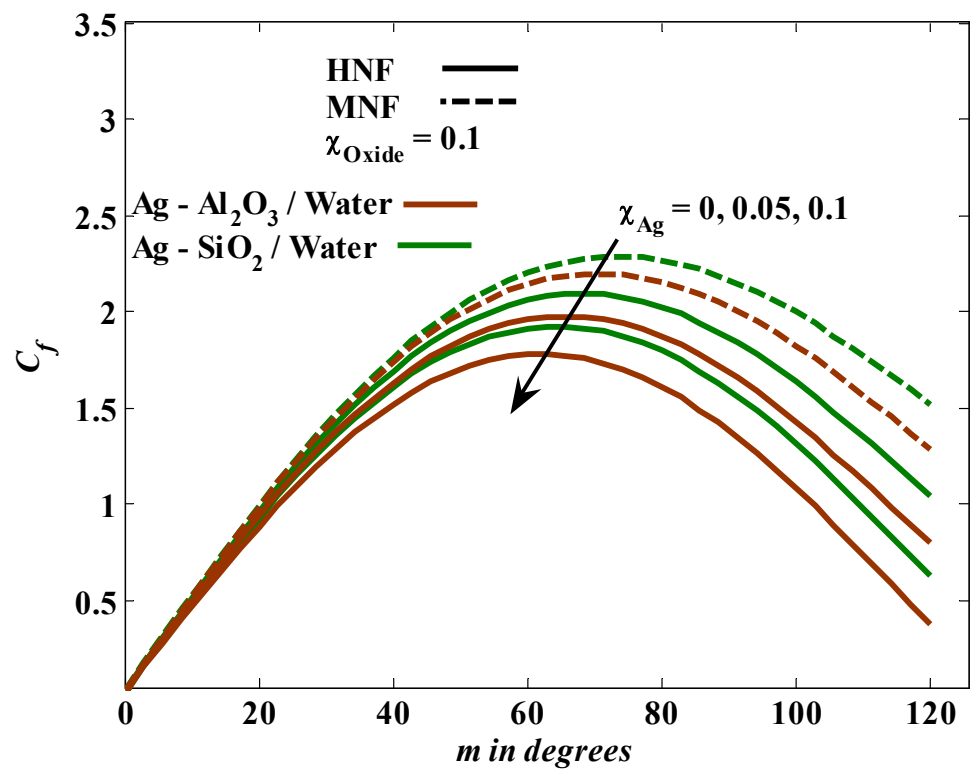

Figure 10. Illustration of χ_{Ag} versus Nusselt number at fixed values of $We = 0.2$, $\lambda = 0.1$, $R = 2$, & $M = 1$.

Figure 11. Illustration of χ_{Ag} versus skin friction at fixed values of $We = 0.2$, $R = 0.1, M = 2, \& \lambda = 1$.

The impact of the thermal radiation factor on temperature and velocity profiles is manifested in Figure 12. Elevating the thermal radiation factor values causes more energy to be imposed inside the Williamson hybrid nanofluid, which raises the velocity and temperature profiles. Figure 13 report the influence of the combined convection parameter on temperature and velocity profiles. It is observed that ascending values of the combined convective factor cause a reduction in the temperature. This also resulted in an improvement in the velocity profiles. In fact, this phenomenon is the result of the enhancement in the buoyant forces due to the increase in the mixed convection values. The effect of rising Weissenberg number values on temperature and velocity is plotted in Figure 14. Intensification in temperatures and curbing in velocity are observed via a higher Weissenberg number. The Weissenberg number is defined as the ratio of relaxation time to retardation time. When the retardation time decreases, an increase in the value of the Weissenberg number occurs, which is accompanied by a decrease in the velocity of the liquid as well as a decrease in the boundary layer thickness. It is clear that the velocity gradient decreases near the surface of the cylinder when the Weissenberg number increases. The increase in this parameter is also accompanied by an increase in the temperature of the host hybrid nanofluid. Figure 15 demonstrate the behavior of both temperature and velocity with the increment in M. Temperature is an increasing map of M, while velocity is a decreasing map of M. This behavior was expected because the increase in the strength of the magnetic field generates a type of force known as the Lorentz force, which raises the temperature of the Williamson hybrid nanofluid fluid and slows it down. In Figure 16, the responses of both temperature and velocity profiles to the increasing volume fraction of the nanosolid are shown. For rising values of the nanosolid volume fraction of Ag, the temperature tends to rise while the reaction velocity is reversed, as its values decrease. The increase in energy transport as χ_{Ag} increases could explain the rising temperature profiles and decreasing velocity. Finally, a noteworthy note made by the results is that regardless of the influencing factors examined in this study, the combination of silver with aluminum

oxide gives water the highest speed, temperature, and energy transfer rate. Furthermore, the Ag-Al$_2$O$_3$/water combination also has the lowest drag forces.
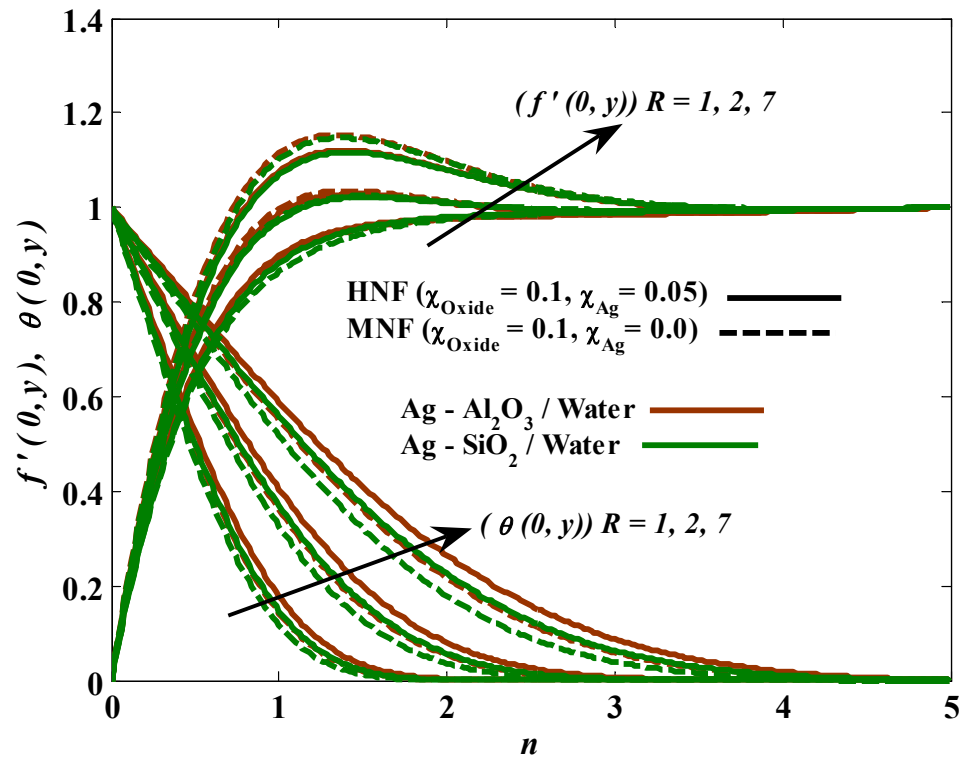

Figure 12. Illustration of R versus temperature and velocity at fixed values of We = 0.2, λ = 0.1, & M = 1.
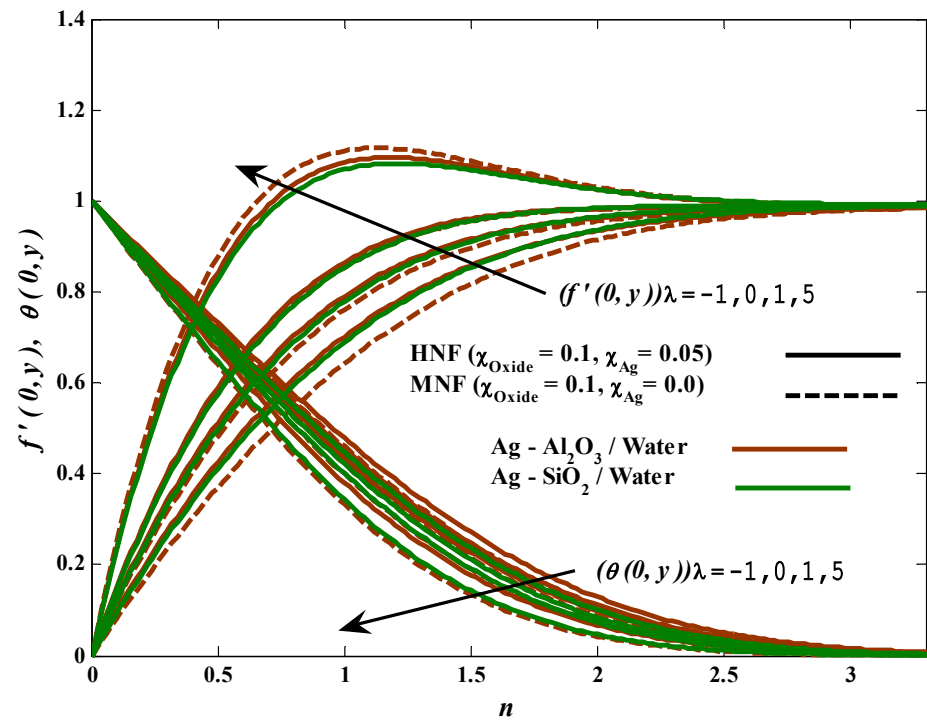

Figure 13. Illustration of λ versus temperature and velocity at fixed values of *We* = 0.2, *R* = 0.1, & M = 1.
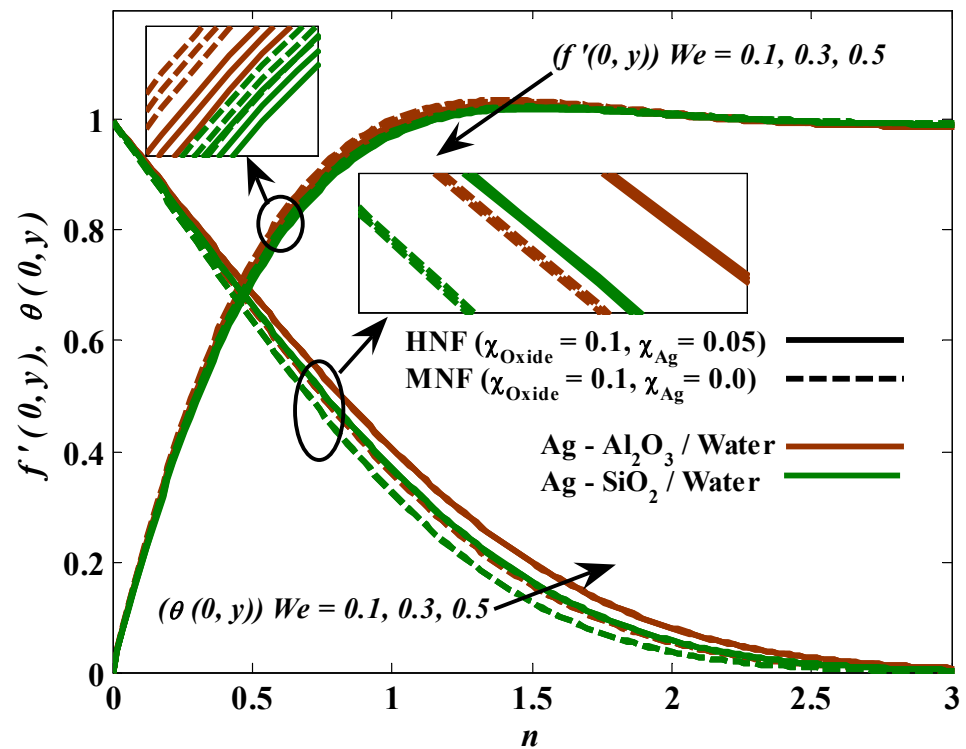
Figure 14. Illustration of *We* versus temperature and velocity at fixed values of $\lambda = 0.2$, $R = 0.1$, & $M = 1$.
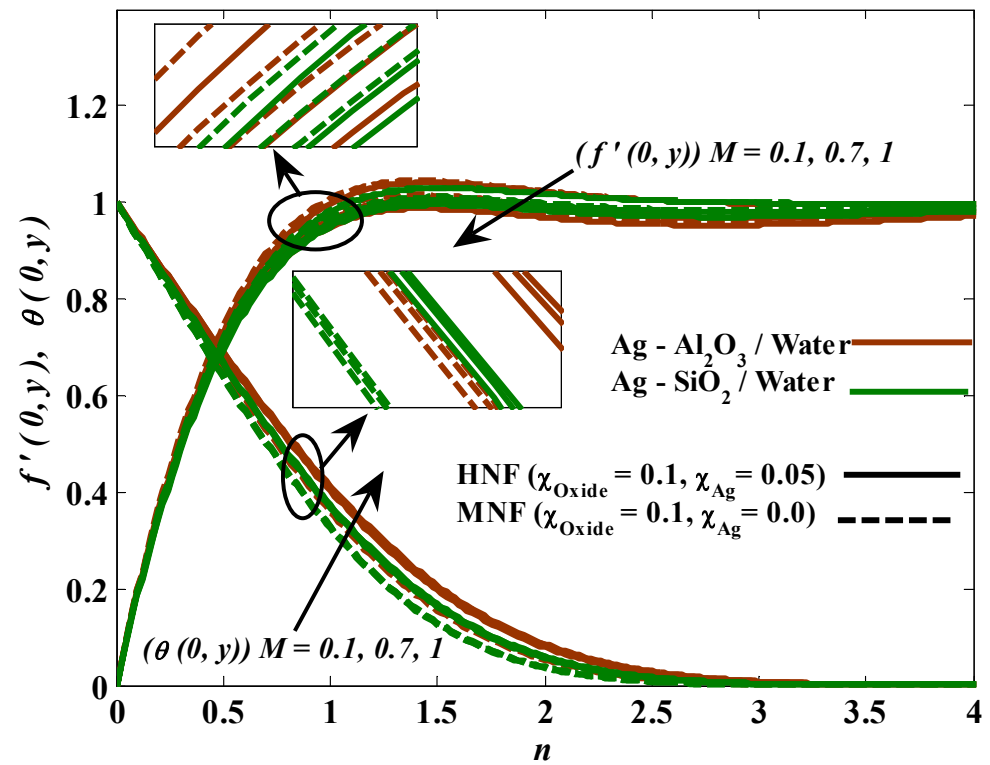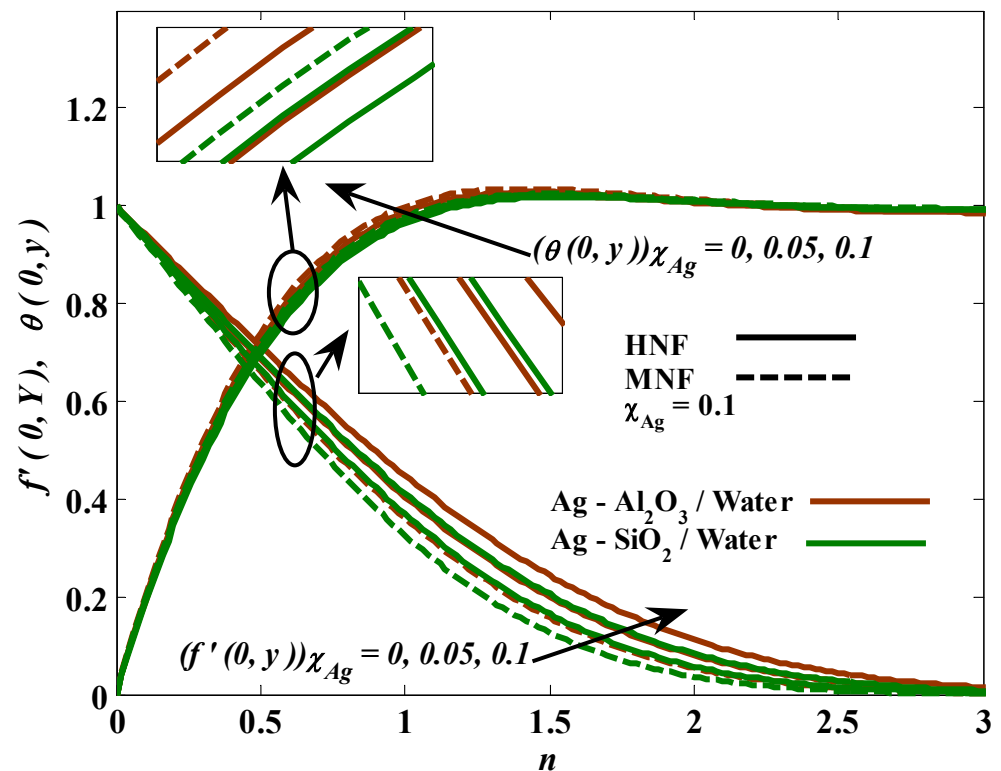

Figure 15. Illustration of *M* versus temperature and velocity at fixed values of $\lambda = 0.2$, $R = 0.1$, & $We = 1$.

Figure 16. Illustration of χ versus temperature and velocity at fixed values of $\lambda = 0.2$, $R = 0.1$, $M = 2$ & $We = 1$.

6. Conclusions

In this analysis, the characteristics of the energy transfer through the Williamson fluid supported by the upgraded nanoparticles were dealt with. The Nanosolid volume fraction χ, combined convection λ, radiation factor R, Weissenberg number We, and magnetic factor M are the factors used to predict the behavior of Williamson hybrid nanofluid, and their ranges are $0 \leq \chi \leq 1$, $-1 \leq \lambda \leq 4$, $0.1 \leq R \leq 6$, $0.2 \leq We \leq 0.9$, and $0.1 \leq M \leq 1$. The following points of significance were drawn:

1. As the magnetic parameter values are increased, the rate of energy transfer, fluid velocity, and drag force decrease while the fluid temperature rises.
2. There is a direct relationship between the parameter of mixed convection on the one hand, and the rate of energy transfer, drag force, and velocity of the host Williamson fluid on the other hand.
3. Thermal radiation positively affects all physical quantities examined in this analysis.
4. Elevating the values of the Weissenberg number causes a curb in velocity, heat transfer rate, and drag forces, as well as an increase in temperature.
5. The nanoparticle combination of silver and aluminum oxide (Ag-Al$_2$O$_3$) has demonstrated superiority in enhancing the energy transfer rate and velocity of the host fluid.

Williamson hybrid nanofluids with combined convection flow under thermal radiation and magnetic effects with boundary conditions such as constant wall temperature was considered. Therefore, there are a lot of potential avenues for future research. For example, ternary hybrid nanofluids, viscous dissipation, and other geometric bodies, such as a solid sphere, stretching sheet, etc., as well as other boundary conditions, such as Newtonian heating.

Author Contributions: Resources, validation, writing—original draft, F.A.A.; Conceptualization, Investigation, writing, review, and editing, F.M.A.F.; Methodology, Software, Investigation, M.Z.S.; Writing, review and editing, investigation, M.A.H.I. All authors have read and agreed to the published version of the manuscript.

Institutional Review Board Statement: Not applicable.

Informed Consent Statement: Not applicable.

Data Availability Statement: Not applicable.

Conflicts of Interest: The authors declare no conflict of interest.

Nomenclature

a	Radius of cylindrical shape	U_∞	uniform free stream
B_o	Magnetic field strength	n	y- component of velocity
C_f	Skin friction coefficient	v_f	Kinematic viscosity sof host liquid
(C_p)	Heat capacity	Greek symbols	
$f(x, y)$	Dimensionless stream function	α	Thermal diffusivity coefficient
g	Gravity vector	β	Thermal expansion of host liquid
Gr	Grashof number	Γ	relaxation time
J	Micro-inertia density	σ	Electrical conductivity
k_f	Thermal conductivity	θ	Temperature of nanoliquid
M	Magnetic parameter	κ	Vortex viscosity
Nu	Nusselt Number	λ	Combined convection parameter
p	Fluid pressure	μ	Dynamic viscosity
Pr	Prandtl number	ρ	Density
Q_R	Rosseland diffusion approximation	ϕ	Spin gradient viscosity
Re	Reynold number	χ	Nano-solid volume fraction
T	Temperature of the fluid	ψ	Stream transformation
T_∞	Ambient temperature		
m	x- component of velocity	Subscript	
$u_e(x)$	free-stream velocity	f	Host liquid
M	Magnetic parameter	nf	Nanoliquid
		s	Nanosolid

References

1. Williamson, R.V. The flow of pseudoplastic materials. *Ind. Eng. Chem.* **1929**, *21*, 1108–1111. [CrossRef]
2. Nadeem, S.; Hussain, S.; Lee, C. Flow of a Williamson fluid over a stretching sheet. *Braz. J. Chem. Eng.* **2013**, *30*, 619–625. [CrossRef]
3. Nadeem, S.; Hussain, S. Heat transfer analysis of Williamson fluid over exponentially stretching surface. *Appl. Math. Mech.* **2014**, *35*, 489–502. [CrossRef]
4. Malik, M.; Bibi, M.; Khan, F.; Salahuddin, T. Numerical solution of Williamson fluid flow past a stretching cylinder and heat transfer with variable thermal conductivity and heat generation/absorption. *AIP Adv.* **2016**, *6*, 035101. [CrossRef]
5. Malik, M.; Salahuddin, T.; Hussain, A.; Bilal, S.; Awais, M. Homogeneous-heterogeneous reactions in Williamson fluid model over a stretching cylinder by using Keller box method. *AIP Adv.* **2015**, *5*, 107227. [CrossRef]
6. Iqbal, W.; Naeem, M.; Jalil, M. Numerical analysis of Williamson fluid flow along an exponentially stretching cylinder. *AIP Adv.* **2019**, *9*, 055118. [CrossRef]
7. Ogunseye, H.; Salawu, S.; Fatunmbi, E. A numerical study of MHD heat and mass transfer of a reactive Casson–Williamson nanofluid past a vertical moving cylinder. *Part. Differ. Equ. Appl. Math.* **2021**, *4*, 100148. [CrossRef]
8. Hussain, S.M.; Jamshed, W.; Pasha, A.A.; Adil, M.; Akram, M. Galerkin finite element solution for electromagnetic radiative impact on viscid Williamson two-phase nanofluid flow via extendable surface. *Int. Commun. Heat Mass Transf.* **2022**, *137*, 106243. [CrossRef]
9. Loganathan, P.; Sangeetha, S. Effect of Williamson parameter on Cu-water Williamson nanofluid over a vertical plate. *Int. Commun. Heat Mass Transf.* **2022**, *137*, 106273. [CrossRef]
10. Almaneea, A. Numerical study on heat and mass transport enhancement in MHD Williamson fluid via hybrid nanoparticles. *Alex. Eng. J.* **2022**, *61*, 8343–8354. [CrossRef]
11. Chol, S.; Estman, J. Enhancing thermal conductivity of fluids with nanoparticles. *ASME-Publ.-Fed* **1995**, *231*, 99–106.

12. Lee, S.; Choi, S.-S.; Li, S.; Eastman, J. Measuring thermal conductivity of fluids containing oxide nanoparticles. *J. Heat Transf. May* **1999**, *121*, 280–289. [CrossRef]

13. Xuan, Y.; Li, Q. Heat transfer enhancement of nanofluids. *Int. J. Numer. Method Heat* **2000**, *21*, 58–64. [CrossRef]

14. Xuan, Y.; Roetzel, W. Conceptions for heat transfer correlation of nanofluids. *Int. J. Heat Mass Transf.* **2000**, *43*, 3701–3707. [CrossRef]

15. Eastman, J.A.; Choi, S.; Li, S.; Yu, W.; Thompson, L. Anomalously increased effective thermal conductivities of ethylene glycol-based nanofluids containing copper nanoparticles. *Appl. Phys. Lett.* **2001**, *78*, 718–720. [CrossRef]

16. Heris, S.Z.; Etemad, S.G.; Esfahany, M.N. Experimental investigation of oxide nanofluids laminar flow convective heat transfer. *Int. Commun. Heat Mass Transf.* **2006**, *33*, 529–535. [CrossRef]

17. Kuznetsov, A.; Nield, D. Natural convective boundary-layer flow of a nanofluid past a vertical plate. *Int. J. Therm. Sci.* **2010**, *49*, 243–247. [CrossRef]

18. Tham, L.; Nazar, R.; Pop, I. Mixed convection boundary layer flow from a horizontal circular cylinder in a nanofluid. *Int. J. Numer. Method Heat* **2012**, *22*, 576–606. [CrossRef]

19. Tham, L.; Nazar, R.; Pop, I. Steady mixed convection flow on a horizontal circular cylinder embedded in a porous medium filled by a nanofluid containing gyrotactic micro-organisms. *J. Heat Transf.* **2013**, *135*, 102601. [CrossRef]

20. Sheremet, M.A.; Pop, I. Natural convection in a horizontal cylindrical annulus filled with a porous medium saturated by a nanofluid using Tiwari and Das' nanofluid model. *Eur. Phys. J. Plus* **2015**, *130*, 1–12. [CrossRef]

21. Dogonchi, A.; Sheremet, M.; Ganji, D.; Pop, I. Free convection of copper–water nanofluid in a porous gap between hot rectangular cylinder and cold circular cylinder under the effect of inclined magnetic field. *J. Anal. Calorim.* **2019**, *135*, 1171–1184. [CrossRef]

22. Alwawi, F.A.; Alkasasbeh, H.T.; Rashad, A.; Idris, R. Heat transfer analysis of ethylene glycol-based Casson nanofluid around a horizontal circular cylinder with MHD effect. *Proc. Inst. Mech. Eng. C. J. Mech. Eng. Sci.* **2020**, *234*, 2569–2580. [CrossRef]

23. Alwawi, F.A.; Hamarsheh, A.S.; Alkasasbeh, H.T.; Idris, R. Mixed Convection Flow of Magnetized Casson Nanofluid over a Cylindrical Surface. *Coatings* **2022**, *12*, 296. [CrossRef]

24. Hamarsheh, A.S.; Alwawi, F.A.; Alkasasbeh, H.T.; Rashad, A.M.; Idris, R. Heat transfer improvement in MHD natural convection flow of graphite oxide/carbon nanotubes-methanol based casson nanofluids past a horizontal circular cylinder. *Processes* **2020**, *8*, 1444. [CrossRef]

25. Sreedevi, P.; Reddy, P.S. Effect of magnetic field and thermal radiation on natural convection in a square cavity filled with TiO_2 nanoparticles using Tiwari-Das nanofluid model. *Alex. Eng. J.* **2022**, *61*, 1529–1541. [CrossRef]

26. Khan, U.; Zaib, A.; Pop, I.; Waini, I.; Ishak, A. MHD flow of a nanofluid due to a nonlinear stretching/shrinking sheet with a convective boundary condition: Tiwari–Das nanofluid model. *Int. J. Numer. Method Heat* **2022**, *32*, 3233–3258. [CrossRef]

27. Jamshed, W.; Kumar, V.; Kumar, V. Computational examination of Casson nanofluid due to a non-linear stretching sheet subjected to particle shape factor: Tiwari and Das model. *Numer. Methods Part. Differ. Equ.* **2022**, *38*, 848–875. [CrossRef]

28. Swalmeh, M.Z.; Shatat, F.; Alwawi, F.A.; Ibrahim, M.A.H.; Sulaiman, I.M.; Yaseen, N.; Naser, M.F. Effectiveness of Radiation on Magneto-Combined Convective Boundary Layer Flow in Polar Nanofluid around a Spherical Shape. *Fractal Fract.* **2022**, *6*, 383. [CrossRef]

29. Swalmeh, M.; Alkasasbeh, H.; Hussanan, A.; Mamat, M. Numerical Study of Mixed Convection Heat Transfer in Methanol based Micropolar Nanofluid about a Horizontal Circular Cylinder. *J. Phys. Conf. Ser.* **2019**, *1366*, 012003. [CrossRef]

30. Leong, K.; Ahmad, K.K.; Ong, H.C.; Ghazali, M.; Baharum, A. Synthesis and thermal conductivity characteristic of hybrid nanofluids–a review. *Renew. Sustain. Energy Rev.* **2017**, *75*, 868–878. [CrossRef]

31. Muneeshwaran, M.; Srinivasan, G.; Muthukumar, P.; Wang, C.-C. Role of hybrid-nanofluid in heat transfer enhancement–A review. *Int. Commun. Heat Mass Transf.* **2021**, *125*, 105341. [CrossRef]

32. Turcu, R.; Darabont, A.; Nan, A.; Aldea, N.; Macovei, D.; Bica, D.; Vekas, L.; Pana, O.; Soran, M.; Koos, A. New polypyrrole-multiwall carbon nanotubes hybrid materials. *J. Optoelectron. Adv. Mater.* **2006**, *8*, 643–647.

33. Suresh, S.; Venkitaraj, K.; Selvakumar, P.; Chandrasekar, M. Synthesis of Al2O3–Cu/water hybrid nanofluids using two step method and its thermo physical properties. *Colloids Surf. A Physicochem. Eng. Asp* **2011**, *388*, 41–48. [CrossRef]

34. Baghbanzadeh, M.; Rashidi, A.; Rashtchian, D.; Lotfi, R.; Amrollahi, A. Synthesis of spherical silica/multiwall carbon nanotubes hybrid nanostructures and investigation of thermal conductivity of related nanofluids. *Thermochim. Acta* **2012**, *549*, 87–94. [CrossRef]

35. Moghadassi, A.; Ghomi, E.; Parvizian, F. A numerical study of water based Al_2O_3 and Al_2O_3–Cu hybrid nanofluid effect on forced convective heat transfer. *Int. J. Therm. Sci.* **2015**, *92*, 50–57. [CrossRef]

36. Mehryan, S.; Izadpanahi, E.; Ghalambaz, M.; Chamkha, A. Mixed convection flow caused by an oscillating cylinder in a square cavity filled with Cu–Al2O3/water hybrid nanofluid. *J. Anal. Calorim.* **2019**, *137*, 965–982. [CrossRef]

37. Aminian, E.; Moghadasi, H.; Saffari, H. Magnetic field effects on forced convection flow of a hybrid nanofluid in a cylinder filled with porous media: A numerical study. *J. Anal. Calorim.* **2020**, *141*, 2019–2031. [CrossRef]

38. Alharbi, S.O.; Nawaz, M.; Nazir, U. Thermal analysis for hybrid nanofluid past a cylinder exposed to magnetic field. *AIP Adv.* **2019**, *9*, 115022. [CrossRef]

39. Patil, P.; Kulkarni, M. Analysis of MHD mixed convection in a Ag-TiO2 hybrid nanofluid flow past a slender cylinder. *Chin. J. Phys.* **2021**, *73*, 406–419. [CrossRef]

40. Alwawi, F.A.; Swalmeh, M.Z.; Qazaq, A.S.; Idris, R. Heat Transmission Reinforcers Induced by MHD Hybrid Nanoparticles for Water/Water-EG Flowing over a Cylinder. *Coatings* **2021**, *11*, 623. [CrossRef]
41. Patil, P.M.; Benawadi, S.; Tonannavar, J.R.; Shanker, B. Homogeneous and heterogeneous reactions in the mixed convection flow of hybrid nanofluid over a slender cylinder. *Asia-Pac. J. Chem. Eng.* **2022**, *17*, e2740. [CrossRef]
42. Sreedevi, P.; Reddy, P.S. Williamson hybrid nanofluid flow over swirling cylinder with Cattaneo–Christov heat flux and gyrotactic microorganism. *Waves Random Complex Media* **2021**, 1–28. [CrossRef]
43. Izady, M.; Dinarvand, S.; Pop, I.; Chamkha, A.J. Flow of aqueous Fe2O3–CuO hybrid nanofluid over a permeable stretching/shrinking wedge: A development on Falkner–Skan problem. *Chin. J. Phys.* **2021**, *74*, 406–420. [CrossRef]
44. Salmi, A.; Madkhali, H.A.; Nawaz, M.; Alharbi, S.O.; Alqahtani, A. Numerical study on non-Fourier heat and mass transfer in partially ionized MHD Williamson hybrid nanofluid. *Int. Commun. Heat Mass Transf.* **2022**, *133*, 105967. [CrossRef]
45. Abderrahmane, A.; Qasem, N.A.; Younis, O.; Marzouki, R.; Mourad, A.; Shah, N.A.; Chung, J.D. MHD Hybrid Nanofluid Mixed Convection Heat Transfer and Entropy Generation in a 3-D Triangular Porous Cavity with Zigzag Wall and Rotating Cylinder. *Mathematics* **2022**, *10*, 769. [CrossRef]
46. Xia, W.-F.; Ahmad, S.; Khan, M.N.; Ahmad, H.; Rehman, A.; Baili, J.; Gia, T.N. Heat and mass transfer analysis of nonlinear mixed convective hybrid nanofluid flow with multiple slip boundary conditions. *Case Stud. Therm. Eng.* **2022**, *32*, 101893. [CrossRef]
47. Khan, U.; Adnan; Haleema, B. Thermal performance in nanofluid and hybrid nanofluid under the influence of mixed convection and viscous dissipation: Numerical investigation. *Waves Random Complex Media* **2022**, 1–19. [CrossRef]
48. Mohammadein, A.; El-Amin, M. Thermal radiation effects on power-law fluids over a horizontal plate embedded in a porous medium. *Int. Commun. Heat Mass Transf.* **2000**, *27*, 1025–1035. [CrossRef]
49. Subba Rao, A.; Amanulla, C.; Nagendra, N.; Beg, O.A.; Kadir, A. Hydromagnetic flow and heat transfer in a Williamson Non-Newtonian fluid from a Horizontal circular cylinder with Newtonian Heating. *Int. J. Appl. Comput. Math.* **2017**, *3*, 3389–3409. [CrossRef]
50. Swalmeh, M.Z.; Alkasasbeh, H.T.; Hussanan, A.; Mamat, M. Influence of micro-rotation and micro-inertia on nanofluid flow over a heated horizontal circular cylinder with free convection. *Theor. Appl. Mech.* **2019**, *46*, 125–145. [CrossRef]
51. Nazar, R.; Amin, N.; Pop, I. Mixed convection boundary-layer flow from a horizontal circular cylinder in micropolar fluids: Case of constant wall temperature. *Int. J. Numer. Method Heat* **2003**, *13*, 86–109. [CrossRef]
52. Howell, J.R.; Mengüç, M.P.; Daun, K.; Siegel, R. *Thermal Radiation Heat Transfer*; CRC Press: Boca Raton, FL, USA, 2020.
53. Dinarvand, S. Nodal/saddle stagnation-point boundary layer flow of CuO–Ag/water hybrid nanofluid: A novel hybridity model. *Microsyst. Technol.* **2019**, *25*, 2609–2623. [CrossRef]
54. Alkasasbeh, H. Numerical solution on heat transfer magnetohydrodynamic flow of micropolar Casson fluid over a horizontal circular cylinder with thermal radiation. *Front. Heat Mass Transf.* **2018**, *10*, 32. [CrossRef]
55. Cebeci, T.; Bradshaw, P. *Physical and Computational Aspects of Convective Heat Transfer*; Springer Science & Business Media: Berlin/Heidelberg, Germany, 2012.
56. Nazar, R.M. *Mathematical Models for Free and Mixed Convection Boundary Layer Flows of Micropolar Fluids*; Universiti Teknologi Malaysia: Johor Bahru, Malaysia, 2004.
57. Swalmeh, M.Z.; Alkasasbeh, H.T.; Hussanan, A.; Mamat, M. Numerical investigation of heat transfer enhancement with Ag-GO water and kerosene oil based micropolar nanofluid over a solid sphere. *J. Adv. Res. Fluid Mech. Therm. Sci.* **2019**, *59*, 269–282.
58. Alwawi, F.A.; Alkasasbeh, H.T.; Rashad, A.M.; Idris, R. Natural convection flow of Sodium Alginate based Casson nanofluid about a solid sphere in the presence of a magnetic field with constant surface heat flux. *J. Phys. Conf. Ser.* **2019**, *1366*, 012005. [CrossRef]